processes

MDPI

Article

Hybrid Solar Photoelectro-Fenton and Ozone Processes for the Sustainable Removal of COVID-19 Pharmaceutical Contaminants

Sonia Herrera-Chávez [1], Martin Pacheco-Álvarez [1,2], Luis A. Godínez [3], Enric Brillas [4] and Juan M. Peralta-Hernández [1,*]

[1] Departamento de Química, División de Ciencias Naturales y Exactas, Universidad de Guanajuato, Cerro de la Venada s/n, Pueblito de Rocha, Guanajuato 36040, Mexico; s.herrerachavez@ugto.mx (S.H.-C.); armando_pache92@outlook.com (M.P.-Á.)
[2] Instituto Tecnológico Superior de Guanajuato, Tecnológico Nacional de México, Carretera Estatal Guanajuato-Puentecillas km 10.5, Guanajuato 36262, Mexico
[3] Centro de Investigación en Química para la Economía Circular (CIQEC), Facultad de Química, Universidad Autónoma de Querétaro, Centro Universitario, Querétaro 76010, Mexico; luis.godinez@uaq.mx
[4] Departament de Ciència de Materials i Química Física, Facultat de Química, Universitat de Barcelona, Martí i Franquès 1-11, 08028 Barcelona, Spain; brillas@ateneu.ub.edu
* Correspondence: juan.peralta@ugto.mx

Abstract

This study explores a hybrid advanced electrochemical oxidation process (EAOP) intensified by solar irradiation and ozone for the treatment of wastewater containing COVID-19-related pharmaceuticals. Pilot-scale trials were performed in a 30 L compound parabolic collector (CPC)-type photoreactor with a boron-doped diamond (BDD–BDD) electrode configuration. Under optimal conditions (50 mg L^{-1} paracetamol, 0.05 M Na_2SO_4, 0.50 mM Fe^{2+}, pH 3.0, and 60 mA cm^{-2}), the solar photoelectro-Fenton (SPEF) process achieved 78% chemical oxygen demand (COD) reduction within 90 min, with catechol and phenol detected as the main aromatic intermediates. When applied to a four-drug mixture (dexamethasone, paracetamol, amoxicillin, and azithromycin), the solar photoelectro-Fenton (SPEF–ozone (O_3)) system reached 60% degradation and 41% COD removal under solar conditions. The results highlight the synergistic effect of ozone and solar energy in enhancing the electrochemical oxidation process (EAOP) performance and demonstrate the potential of these processes for scalable and sustainable removal of pharmaceutical contaminants from wastewater.

Keywords: COVID-19 pharmaceuticals; drug degradation; solar photoelectro-Fenton (SPEF); ozone-assisted EAOPs; wastewater treatment

Academic Editor: George Z. Kyzas

Received: 9 September 2025
Revised: 3 October 2025
Accepted: 9 October 2025
Published: 10 October 2025

Citation: Herrera-Chávez, S.; Pacheco-Álvarez, M.; Godínez, L.A.; Brillas, E.; Peralta-Hernández, J.M. Hybrid Solar Photoelectro-Fenton and Ozone Processes for the Sustainable Removal of COVID-19 Pharmaceutical Contaminants. *Processes* **2025**, *13*, 3234. https://doi.org/10.3390/pr13103234

1. Introduction

In December 2019, a novel coronavirus disease (COVID-19), caused by the Severe Acute Respiratory Syndrome coronavirus 2 (SARS-CoV-2), rapidly spread worldwide [1]. Since the emergence of COVID-19, the most important challenge for researchers and healthcare professionals has been to find the best treatment options for the new disease. In this regard, the World Health Organization published general guidelines to deal with the SARS-COV-2 disease, which included palliative care [2,3]. To combat this threat, anti-inflammatory drugs have emerged as a symptomatic treatment option for COVID-19. The use of anti-inflammatory drugs such as paracetamol and ibuprofen is currently considered

one of the most effective approaches for the treatment of the symptoms of COVID-19 [4,5]. In this regard, related studies have shown that up to 85% of COVID-19 patients develop fever, and paracetamol is commonly used as the first treatment [6].

Despite the high importance of these drugs for COVID-19 patients, one aspect that must be considered is the environmental impact that these chemical substances are causing upon disposal. In this way, after being administered to patients, a variable proportion of these chemicals have been detected in effluents, wastewater plants, and even in surface and underground water bodies that, at some point in time, are recharged with treated water [7]. The most frequently employed cocktail of drugs used for the symptomatic treatment of COVID-19 includes different medications that depend on the location in which the medical treatment takes place. In this regard, Table 1 summarizes some of the most commonly used drugs whose consumption became popular during the COVID-19 pandemic, along with some of their physicochemical properties [8]. Further information is provided in Figures S1–S3.

Table 1. CAS Registry Number, Molecular Formula, and Molecular Weight, and Water Solubility of Some Drugs Used During the COVID-19 Pandemic.

Drug	CAS	Molecular Formula	Molecular Weight	Solubility in Water (mg (100 mL)$^{-1}$)
Paracetamol	103-90-2	$C_8H_9NO_2$	151.16 g mol^{-1}	1.4
Dexamethasone	50-02-2	$C_{22}H_{29}FO_5$	392.46 g mol^{-1}	1000
Azithromycin	83905-01-05	$C_{38}H_{72}N_2O_{12}$	749 g mol^{-1}	514
Amoxicillin	26787-78-0	$C_{16}H_{19}N_3O_5S$	365.4 gmol^{-1}	10.7

The presence of pharmaceuticals in the environment, such as paracetamol, is mainly due to their incomplete removal during wastewater treatment and inadequate management, leading to their persistence in treated effluents and eventual discharge into surface waters.

According to previous studies, the concentration of paracetamol in natural water bodies varies widely around the world due to factors such as local consumption habits, the effectiveness of wastewater treatment systems, and various environmental conditions [9,10]. The problem arises since some chemical substances, such as hydroquinone, p-aminophenol, n-acetyl-benzoquinone, and 1,4-benzoquinone, are often intermediates with high liver toxicity. In this context, paracetamol concentrations ranging from 1 to 100 μg L^{-1} have been detected in wastewater in countries such as Korea, Spain, and the Western Balkans, raising concerns about the potential ecological impacts on aquatic life, long-term accumulation, emergence of resistance, and human exposure through water consumption. Despite this situation, many countries lack specific regulations on permitted levels of paracetamol discharge, particularly in areas close to pharmaceutical plants [11].

During the COVID-19 pandemic, efforts focused on mitigating the number of fatalities and trying to provide early treatment to individuals in "at-risk groups". In 2020, during the health crisis, the use of different non-antiviral drugs also became popular [12], and their presence and that of their related by-products have become an important environmental issue. In this context, over the previous three decades, Advanced Oxidation Processes (AOPs) have been identified as options for removing organic compounds from wastewater and water bodies. These processes include a variety of chemical, photochemical, electrochemical, and photoelectrochemical methods where organic compounds are oxidized and frequently mineralized due to the attack of reactive oxygen species (ROS) [13,14].

Electrochemical Advanced Oxidation Processes (EAOPs) constitute a subgroup within advanced oxidation processes that have demonstrated high efficiency in removing persistent and toxic pollutants from wastewater, mainly due to their ability to generate strong oxidizing species under relatively mild operating conditions [15]. Among them, anodic oxi-

dation (AO) represents the most straightforward approach, in which organic contaminants are degraded through direct electron transfer or via hydroxyl radicals (M(•OH)) weakly adsorbed on the surface of the anode (M), as expressed in Equation (1) [16]. Common electrode materials used for this purpose are boron-doped diamond (BDD) and dimensionally stable anodes (DSA). Another frequently applied strategy is the electro-Fenton (EF) process, which involves the cathodic generation of hydrogen peroxide (H_2O_2) through Equation (2), followed by its reaction with added Fe^{2+} ions to produce hydroxyl radicals (•OH) via the classical Fenton reaction (Equation (3)) [17,18]. The Fe^{2+} consumed in this process can be continuously regenerated by cathodic reduction of Fe^{3+}, according to Equation (4). Contaminants are thus eliminated by a combination of direct anodic oxidation, mediated oxidation through M(•OH), and homogeneous •OH attack. Nevertheless, the EF process often achieves limited mineralization due to the persistence of stable Fe(III)-carboxylate complexes ($Fe(OOCR)^{2+}$), which are poorly reactive towards •OH [19,20]. To overcome this limitation, irradiation with UV light has been introduced, leading to the photoelectro-Fenton (PEF) process, which significantly enhances mineralization efficiency [21]. In particular, the use of sunlight as an irradiation source (solar PEF, SPEF) provides an attractive and sustainable option, since it promotes the photolysis of $Fe(OH)^{2+}$ complexes (Equation (5)) to regenerate Fe^{2+} and produce additional •OH, as well as the photodecomposition of Fe(III)-carboxylates (Equation (6)), thereby improving overall pollutant removal.

$$M + H_2O \rightarrow M(^{\bullet}OH) + H^+ + e^- \quad (1)$$

$$O_2 + 2H^+ + 2e^- \rightarrow H_2O_2 \quad (2)$$

$$Fe^{2+} + H_2O_2 \rightarrow Fe^{3+} + {}^{\bullet}OH + OH^- \quad (3)$$

$$Fe^{3+} + e^- \rightarrow Fe^{2+} \quad (4)$$

$$Fe(OH)^{2+} + hv \rightarrow Fe^{2+} + {}^{\bullet}OH \quad (5)$$

$$Fe(OOCR)^{2+} + hv \rightarrow Fe^{2+} + CO_2 + R^{\bullet} \quad (6)$$

In contrast, it is widely recognized that the application of ozone alone often results in a relatively slow degradation of pollutants in wastewater, mainly because this process produces limited amounts of hydroxyl radicals (•OH), which are far more powerful oxidants [22]. However, when ozone treatment is combined with ultraviolet (UV) irradiation, the oxidative efficiency of the system is markedly improved. In aqueous solution, ozone exhibits a maximum molar absorption coefficient (εmax) of 3600 $L \cdot mol^{-1} \cdot cm^{-1}$ at a wavelength of 253.7 nm. Under these conditions, ozone molecules can be photoactivated by solar UV light, enabling their reaction with water to generate hydrogen peroxide (H_2O_2) according to Equation (7). Subsequently, H_2O_2 can undergo reduction, giving rise to homogeneous hydroxyl radicals (•OH) as described by Equation (8) [23,24].

$$O_3 + H_2O + hv \rightarrow H_2O_2 + O_2 \quad (7)$$

$$H_2O_2 + O_2 \rightarrow 2{}^{\bullet}OH + 3O_2 \quad (8)$$

The purpose of this research is to establish an effective solar photoelectro-Fenton system coupled with ozone (SPEF/O_3) for the treatment of wastewater contaminated with pharmaceuticals commonly prescribed during the symptomatic management of COVID-19. Since wastewater containing these compounds represents a complex chemical matrix, a methodological approach was employed not only to assess the overall efficiency of the process but also to identify and characterize the main transformation products. Previous studies have already demonstrated the feasibility of using the solar photoelectro-Fenton process with CPC-type photoreactors for the degradation of industrial anilines [25]. Build-

ing on this knowledge, the present work first evaluates paracetamol as a model contaminant under SPEF conditions. Subsequently, the comparative removal of a representative drug mixture—dexamethasone, paracetamol, azithromycin, and amoxicillin—was investigated by both O_3/sunlight and SPEF/O_3 processes. The selection of these four pharmaceuticals responds to their massive use during the COVID-19 pandemic, which led to their recognition as emerging pollutants of major environmental concern. The experimental assays were carried out in a pilot setup consisting of a filter-press electrochemical cell with BDD/BDD electrodes connected to a CPC-type photoreactor and integrated with an ozone generator. In addition, the abatement of chemical oxygen demand (COD) and the formation of key intermediates were quantified to evaluate process performance.

This research is framed within a pressing global challenge: the post-pandemic contamination caused by the extensive use of pharmaceuticals. The persistent detection of these compounds in aquatic ecosystems has been documented in several countries, including Mexico, the site of the present study. To the best of our knowledge, this is the first report in Latin America that evaluates the combined application of solar photoelectro-Fenton (SPEF) and ozonation for the removal of post-COVID-19 pharmaceuticals at a pilot scale under natural solar irradiation.

The technological approach proposed here addresses an emerging environmental problem through a sustainable strategy, as it relies on solar energy—an abundant, free, and renewable resource. Furthermore, the system is based on commercially available components (BDD electrodes, ozone generator, and CPC photoreactors), which enhances its potential for replication in developing countries. This configuration demonstrates technical feasibility for large-scale applications, enabling the simultaneous degradation of diverse pharmaceuticals—such as antibiotics, anti-inflammatory agents, and corticosteroids—in complex water matrices. Such integrative treatment represents a significant step forward compared to prior studies that have mainly focused on the degradation of single compounds.

2. Experimental Section

2.1. Chemicals

Commercial dexamethasone, paracetamol, amoxicillin, and azithromycin were obtained from a drug store in Mexico (Farmacias del Ahorro, Mexico City, Mexico). Analytical grade sodium sulfate (Na_2SO_4), used as a supporting electrolyte, was purchased from Karal (Gto, México). Analytical grade heptahydrated iron (II) sulfate ($FeSO_4 \cdot 7H_2O$) for Fenton-based processes and analytical grade sulfuric acid for adjusting the solution pH to 3.0 were obtained from J.T. Baker™ (Radnor, PA, USA). All other chemicals used for high-performance liquid chromatography (HPLC) were purchased from Sigma-Aldrich (Saint Louis, MO, USA). The solutions used for this work were prepared using raw water, whose physicochemical characteristics are shown in Table 2.

Table 2. Physicochemical Characterization of the Raw Water Used in this Study.

Parameter	Value
Total dissolved solids (TDS)	232 mg L^{-1}
Temperature	23–25.5 °C
Salinity	0.042%
Specific density	1.100
pH	7.1
Oxidation-Reduction Potential (ORP)	143–154 mV
Electrical conductivity (EC)	480 μS cm^{-1}
Total hardness	78.05 mg L^{-1}
Hardness to Mg	19.5 mg L^{-1}
Hardness to Ca	58.1 mg L^{-1}

2.2. Electrochemical Set-Up

Figure 1 depicts the batch SPEF/O_3 pilot plant employed in this study, consisting of the following components: (1) a filter-press electrochemical cell, (2) a CPC-type photoreactor, (3) an ozone generator, (4) a DC power supply, (5) a storage reservoir, and (6) a centrifugal pump. The system was specifically configured to treat 30 L of aqueous solution, either containing paracetamol or a mixture of pharmaceuticals. The solution was kept in a plastic storage tank and continuously circulated through the plant using a centrifugal pump, maintaining a flow rate of 300 L h^{-1} to ensure homogeneous mixing and efficient contact with all treatment units.

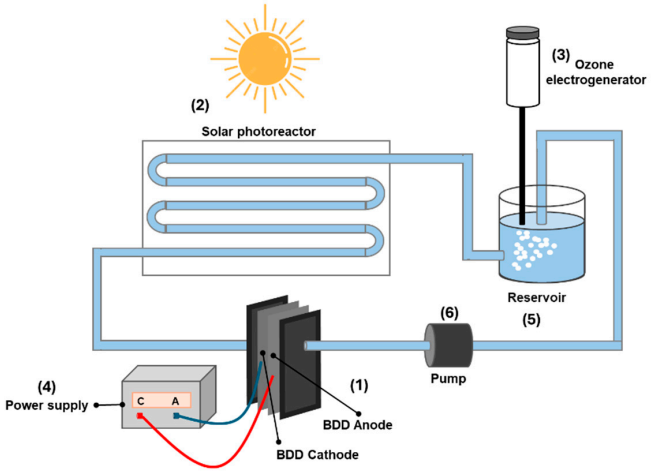

Figure 1. Assembly of a CPC-type continuous flow reactor coupled with ozone. (1) filter press-type electrochemical cell, (2) CPC-type reactor, (3) ozone generator, (4) power supply, (5) reservoir, and (6) centrifugal pump.

The operating temperature was controlled at 27 °C by means of two heat exchangers. The electrochemical system employed a filter-press reactor fitted with boron-doped diamond (BDD) electrodes (anode and cathode, 64 cm^2 each, Metakem™, Metakem GmbH, Usingen, Germany). Aeration was achieved through a cascade induced by the water flow, which guaranteed oxygen saturation and, consequently, the continuous electrogeneration of H_2O_2 at the BDD cathode. The electrode gap was fixed at 1.5 cm, and to enhance hydrodynamic conditions and favor mass transfer, a turbulence promoter was inserted into the cell.

For the solar irradiation stage, a compound parabolic collector (CPC) photoreactor was used, consisting of DURAN® glass tubes,15 L total capacity (AO Sol, Carnaxide, Portugal). This configuration allowed an efficient concentration of solar light with a factor close to unity, owing to the arrangement of the parallel tubular modules. The tubes were mounted on aluminum supports over an inclined platform set at 20°, corresponding to the latitude of the experimental site in Mexico, to maximize solar radiation capture.

The solar photoelectro-Fenton (SPEF) assays were conducted during the summer of 2024, exclusively under sunny conditions. The intensity of natural UV-A radiation (300–400 nm) ranged between 30 and 35 W m^{-2}, as determined with a Kipp & Zonen CUV 5 radiometer (OTT HydroMet Corp., Sterling, VA, USA). The electrochemical cell was powered by a B.K. Precision 1688B DC supply, applying continuous current densities (j) of 20, 40, and 60 mA cm^{-2}. Each experimental run lasted 90 min, since longer treatment times were associated with a marked decrease in solar irradiance [25].

Before the trials, the BDD electrodes underwent a cleaning and activation protocol by applying j = 100 mA cm^{-2} in a 0.05 M Na_2SO_4 solution for 120 min, ensuring optimal electrochemical performance throughout the experiments.

When O_3 alone (without passing current) and the combined SFEF/O_3 system were used, the O_3 gas was generated from dry air in an ozone generator provided by Ozone Carbar's Inc. (Gto, México), with a maximum capacity of 7 L min^{-1}. O_3 was supplied to the solution through a glass diffuser, employing a Teflon connection from the ozone generator to the CPC-type photoreactor. The O_3 concentration in the solution was determined by the standard iodometric method (APHA, AWWA, and WPCF; 1995). These experiments were carried out at room temperature and in batch mode by continuously recirculating the solution and bubbling O_3 into it.

2.3. Analytical Measurements

2.3.1. High-Performance Liquid Chromatography (HPLC) Methodology

Chromatographic assays were performed on an Agilent 1260 Infinity HPLC (Agilent Technologies, Inc., Santa Clara, CA, USA) with a diode array UV detector and a Supelco C18 column (25 cm × 4.6 mm) with a 5 µm particle size (Merck KGaA, Darmstadt, Germany). All chemicals used were of pharmaceutical grade, and solvents were of HPLC grade. From a stock solution of paracetamol at 50 mg L^{-1} in the mobile phase, working standard solutions were prepared by dilution in a range of 10–50 mg L^{-1}. A 10 µL aliquot of each solution was injected into the column, and the chromatograms were recorded at λ = 245 nm. Similar conditions were made to standardize the mixture of drugs and that of the intermediates catechol and phenol at λ = 245 nm.

Table 3 shows the working conditions for the determination of paracetamol concentration in water. For this, the samples were injected after a simple pretreatment by solid phase extraction (SPE) with a Millex cartridge (Merck KGaA, Darmstadt, Germany) with a 0.45 µm Nylon membrane, a volume of 500 µL of solvent was eluted to activate the column, followed by 2 mL of the aliquots taken at different electrolysis times. Once the samples were obtained without salts, the filtered solutions were stored in vials at room temperature until their analysis. The amount of active ingredients was quantified by comparing the peak area with the concentration vs. absorbance regression previously obtained.

Table 3. Conditions for Determinations by High-Performance Liquid Chromatography Methodology.

Column	**Supelco C_{18} (25 cm × 4.6 mm), 5 µm**
Wavelength	245 nm
Mobile phase	Water: Acetonitrile
Retention time	5.258 min
Flow rate	1 mL min^{-1}
Temperature	25 °C
Injection volume	10 µL

The decay of drug concentration under different electrolysis conditions was calculated from Equation (9) [26]:

$$\%\text{Degradation} = \frac{\Delta c}{c_0} 100 \quad (9)$$

where Δc is the decay of drug concentration expressed (in mg L^{-1}) at the electrolysis time t (in min), and c_0 corresponds to the initial concentration.

2.3.2. Hydrogen Peroxide (H_2O_2) Electrogeneration/Accumulation

The concentration of accumulated H_2O_2 during the trials was determined by UV-Vis titration with titanium (IV) oxysulfate [$Ti(SO_4)_2$] at λ = 407 nm [27]. The Faradaic efficiency η in (%) of H_2O_2 accumulation is described by Equation (10):

$$\eta = \frac{n\ F\ [H_2O_2]\ V_s}{I\ t} 100 \quad (10)$$

where n is the number of electrons required for O_2 reduction to H_2O_2 production. F is the Faraday constant (96, 500 C mol^{-1}), $[H_2O_2]$ is the H_2O_2 concentration (in M), V_s is the solution volume (in L), I is the current intensity (in A), and t is the reaction time (in s).

2.3.3. Chemical Oxygen Demand (COD) Analysis

The estimation of the quantity of oxidizable material through chemical oxygen demand (COD) assays was followed by the 5220D method outlined in Standard Methods. The specific energy consumption per unit COD mass (EC_{COD}) at time t (in h) for each trial was calculated from Equation (11).

$$EC_{COD}(kWh(g\ COD)^{-1}) = \frac{2.7 \times 10^{-7} E_{cell}\ I\ t}{V_s\ \Delta(COD)} \quad (11)$$

where E_{cell} is the average potential difference in the cell (in V), t is the electrolysis time (in h), and Δ(COD) is the decrease in COD at time t (in mg O_2 L^{-1}).

All the assays were performed in triplicate, reporting the average data with a 95% confidence interval in the figures of merit.

3. Results and Discussion

3.1. Solar Radiation

Figure 2 illustrates the variation in solar radiation intensity over time during the illumination of the CPC-type photoreactor. The experimental data were fitted to a polynomial regression model (R^2 = 0.9518) obtained during a representative SPEF track. The results show that the maximum solar irradiance occurred between 75 and 90 min of electrolysis, followed by a gradual decrease until reaching its minimum value at 240 min. This trend was consistent with the temperature evolution of the system, which increased from 24.5 to 29 °C, as recorded by the nearest Automatic Meteorological Station (EMAS) to the experimental site.

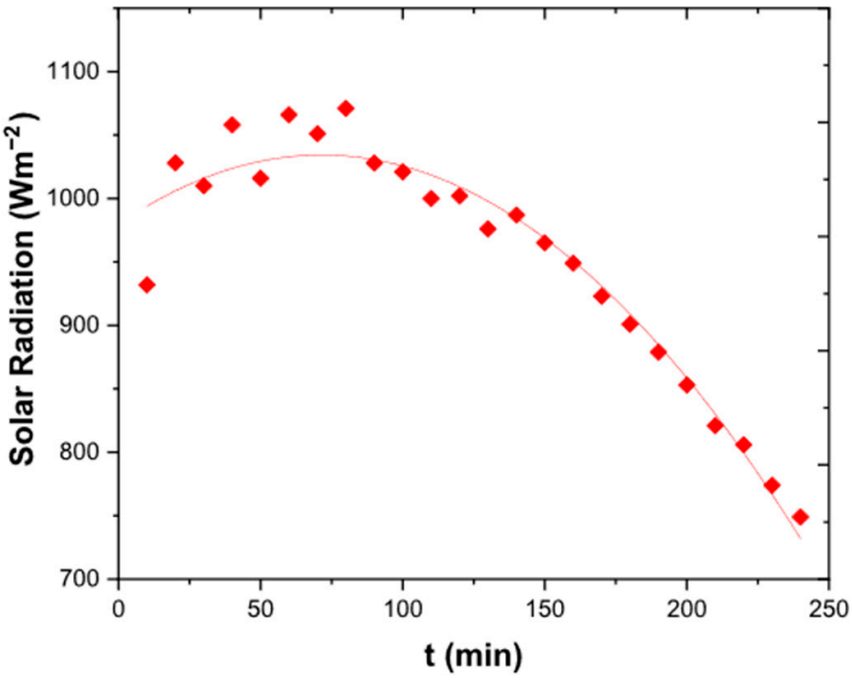

Figure 2. The course of radiation during electrochemical treatment. Coordinates: 21°1′35.45″ N, 101°16′10.98″ E.

This observation highlights the potential to couple the photoreactor with photovoltaic cells in future applications, enabling estimation of the energy conversion efficiency of the system. Based on the irradiance profile, an operational time of 90 min was established as the standard electrolysis duration for each experimental day.

3.2. Electrogeneration of Hydrogen Peroxide at Solar CPC Photoreactor

Hydrogen peroxide (H_2O_2) is a highly versatile chemical agent, characterized by a relatively low oxidizing strength due to its standard reduction potential (E° = 1.763 V/SHE) [28]. The electrogeneration of H_2O_2 at the cathode in electrochemical systems is mainly influenced by factors such as the applied current density (j), the nature of the electrode material, and the operational mode of the process.

In this work, the objective was to assess the in-situ production of H_2O_2 at pilot scale, coupled with a CPC-type photoreactor, with the purpose of achieving high Faradaic efficiency and thereby minimizing the specific energy consumption, depending on both the electrode surface area and the SPEF operating conditions. For this purpose, a BDD/BDD electrode configuration (64 cm^2 geometric area each) was employed to treat a 30 L solution, continuously recirculated at 300 L h^{-1}. The supporting electrolyte consisted of 0.5 M Na_2SO_4, and the experiments were carried out under constant current densities of 20, 40, and 60 mA cm^{-2} [29].

Figure 3a shows the evolution of H_2O_2 accumulation in the solution as a function of the applied current density (j). The increase in j enhanced the reduction in O_2 at the BDD cathode (Equation (2)), thereby promoting higher concentrations of electrogenerated H_2O_2. At j = 20 mA cm^{-2} (●), the concentration reached 2.21 mM after 60 min of polarization, whereas at j = 40 mA cm^{-2} (■), a slightly higher value of 2.43 mM was obtained. In contrast, the application of j = 60 mA cm^{-2} (▲) favored an accumulation close to 3.0 mM.

The accumulation profile revealed a nearly linear increase during the first 30 min of electrolysis, followed by the onset of a plateau. This behavior can be attributed to the dynamic equilibrium between the continuous electrogeneration of H_2O_2 and its parallel loss processes. The main causes of H_2O_2 depletion are: (i) its anodic oxidation, yielding the weaker physisorbed hydroperoxyl radical ($M(HO_2^\bullet)$) (Equation (12)), and (ii) its spontaneous chemical decomposition into H_2O and O_2 (Equation (13)) [30].

$$M + H_2O_2 \rightarrow M(HO_2^\bullet) + H^+ + e^- \quad (12)$$

$$H_2O_2 \rightarrow H_2O + O_2 \quad (13)$$

The evaluation of Faradaic efficiency (η) provides insight into the relationship between the amount of accumulated H_2O_2 and the corresponding electrical charge consumed during the electrochemical process. The η values were calculated according to Equation (10), under the assumption that n = 2, i.e., that the only cathodic reaction taking place is described by Equation (2).

As illustrated in Figure 3b, η decreased progressively with increasing current density (j), ranging from 52% to 27% at the initial stages of electrolysis for j = 20 mA cm^{-2} (●), 40 mA cm^{-2} (■), and 60 mA cm^{-2} (▲). At longer electrolysis times, η exhibited a gradual decay for all conditions, mainly attributed to the enhancement of H_2O_2 decomposition pathways (Equations (12) and (13)) as its concentration increased in the medium.

Although higher current density was associated with lower Faradaic efficiency, the condition of j = 60 mA cm^{-2} was selected for subsequent experiments, since it led to the highest H_2O_2 production, ensuring greater availability of oxidizing species for the SPEF process.

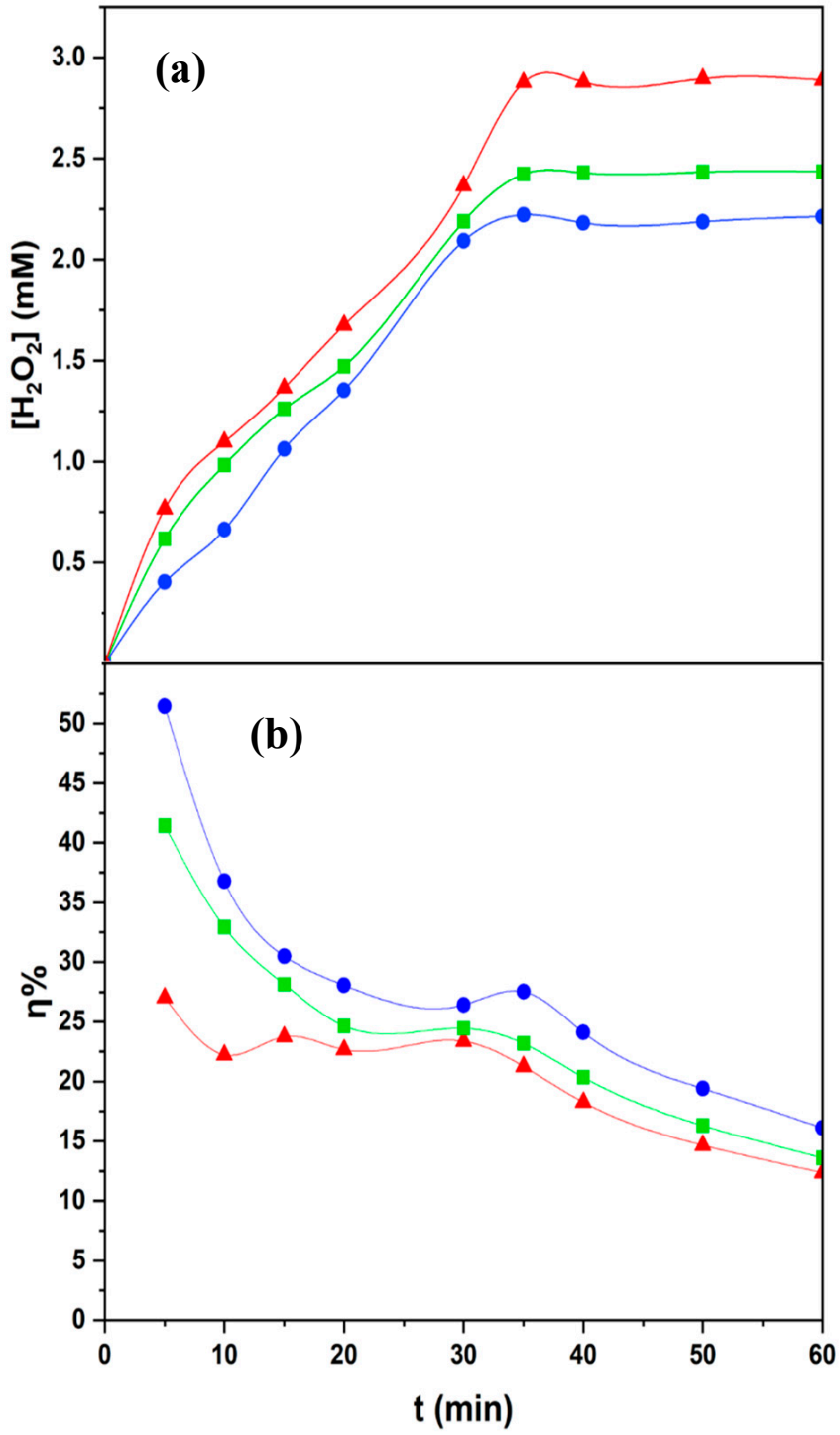

Figure 3. (**a**) Accumulation of H_2O_2 to electrolysis time at current density (*j*): (●) 20, (■) 40, and (▲) 60 mA cm^{-2}. Continuous recirculation flows at 300 L h^{-1} using 0.5 M Na_2SO_4 as the supporting electrolyte and 30 L volume. (**b**) Faradaic current vs. electrolysis time for the above assays.

3.3. Degradation of Paracetamol with CPC-Type Photoreactor by SPEF Process

The experiments evaluated the degradation of 30 L solutions containing 20 mg L^{-1} of paracetamol with 0.05 mM Na_2SO_4 and 0.5 mM Fe^{2+} at pH 3.0, 27 °C, and j = 60 mA cm^{-2}. Paracetamol was chosen as a model pollutant due to its global consumption, frequent detection in wastewater, and increased use during the COVID-19 pandemic; therefore, studying paracetamol under typical electrochemical oxidation conditions provides a reliable benchmark to assess process efficiency and applicability at pilot-plant scale.

As a preliminary test, direct photolysis of the solution without Fe^{2+} and current applied was carried out to evaluate the capacity of the action of sunlight to photolyze the drug. The paracetamol concentration was monitored by HPLC, as explained in Section 2.

Figure 4 demonstrates that direct photolysis alone was ineffective for the degradation of paracetamol, since after 90 min of irradiation, only about 10% of the initial concentration was removed (●). This confirms the strong photostability of paracetamol and the need for more advanced oxidation methods.

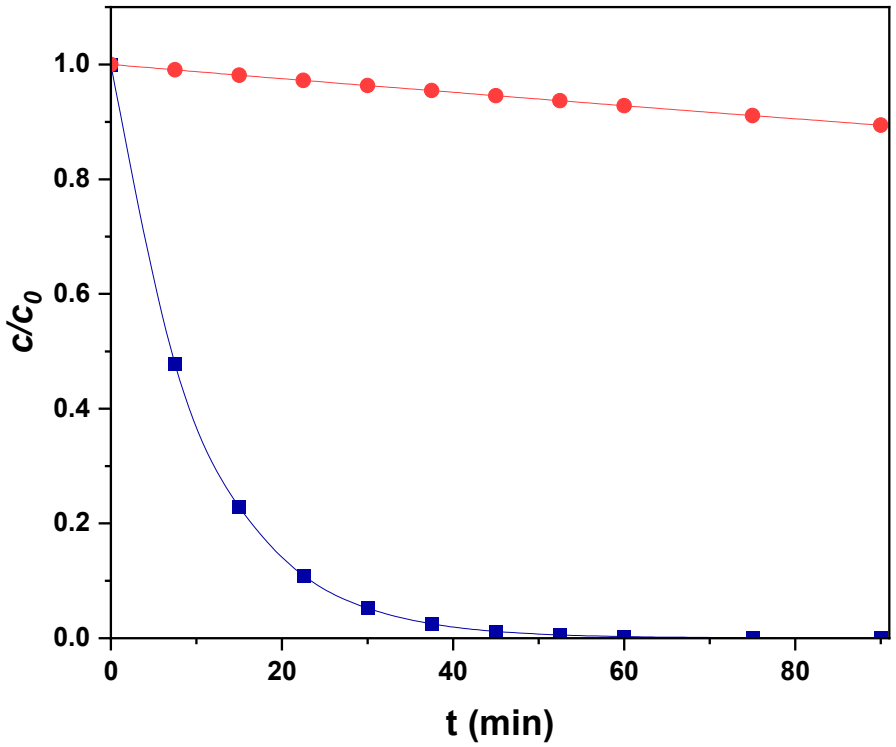

Figure 4. Normalized concentration for 20 mg L^{-1} of paracetamol by direct photolysis (●) and solar photoelectro-Fenton (SPEF) processes (■) in a CPC-type reactor of 30 L and liquid flow rate of 300 L h^{-1}. In all the tests, 0.05 mM Na_2SO_4 was used as the supporting electrolyte by adding 0.5 mM Fe^{2+} at j = 60 mA cm^{-2}.

In contrast, the application of SPEF with 0.5 mM Fe^{2+} (■) led to the complete degradation of the drug within approximately 50 min, underscoring the high efficiency of electrogenerated hydroxyl radicals, particularly when their production is enhanced by natural solar irradiation. The process relies on the synergistic action between electrochemically generated H_2O_2, the catalytic role of Fe^{2+} ions, and the additional contribution of solar photons.

Figure 5 illustrates the chromatographic evolution of paracetamol during its oxidation by the SPEF process. At the onset of treatment, the compound exhibited a well-defined chromatographic peak with a retention time of 2.25 min. As the reaction progressed, this peak progressively decreased in intensity, reflecting the continuous degradation of the pharmaceutical. After approximately 80 min of electrolysis, the paracetamol signal had virtually disappeared, in full agreement with the degradation profile reported in Figure 4 (■).

These results provide further confirmation of the high efficiency of the SPEF process at pilot scale, demonstrating its ability to achieve the complete elimination of paracetamol from aqueous matrices under the tested conditions.

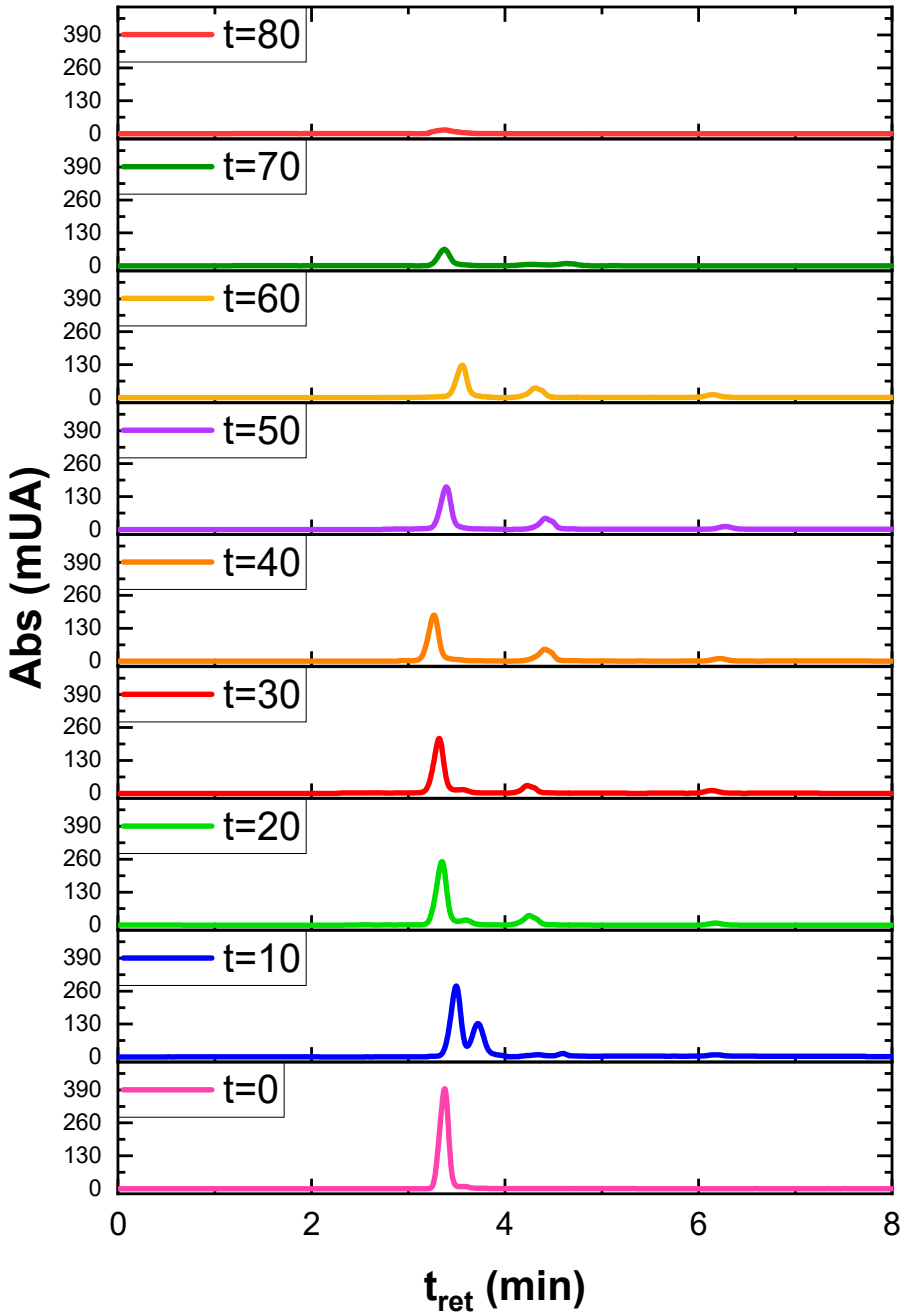

Figure 5. Chromatographic analysis of the decrease in the concentration of 20 mg L^{-1} of paracetamol under the oxidative action of the SFEF process in Figure 4.

3.4. Identification of Intermediates

It is known that paracetamol undergoes oxidation processes, giving rise to intermediate compounds mainly polyphenols, including catechol, aminophenol, and resorcinol, among others [31–33]. In the SPEF process, the HPLC analysis confirmed the formation of aromatic intermediates from the first 10 min of electrolysis. Two main intermediates were detected: catechol (■), which reached 3.25 mg L^{-1} at 10 min and disappeared by 60 min, and phenol (●), which peaked at 2.40 mg L^{-1} at 30 min before being completely degraded by the end of the process, as can be seen in Figure 5. This trend can be observed in their concentration vs. electrolysis time plots shown in Figure 6. It is important to highlight that paracetamol, as well as its transformation aromatic by-products, can be successfully degraded after a total reaction time of 80 min, as similarly found for other drugs [34].

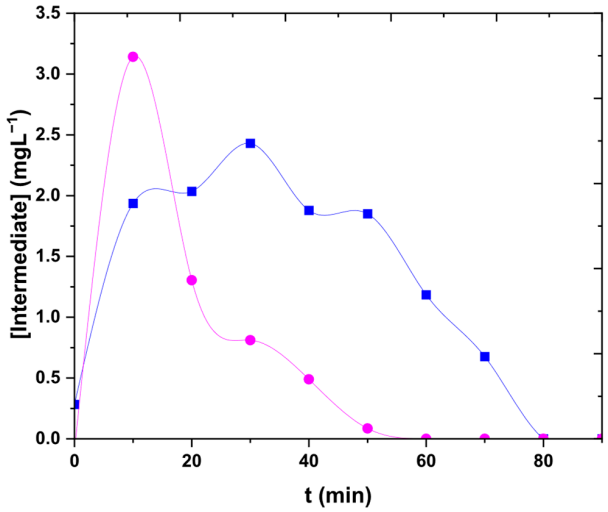

Figure 6. The time course of the evolution of intermediates during the decrease of 20 mg L^{-1} of paracetamol is shown in Figure 5. Catechol (■) and Phenol (●).

3.5. Cyclic Voltammetric Analysis

Figure 7 presents the cyclic voltammograms obtained for a 20 mg L^{-1} paracetamol solution, recorded at a scan rate of 100 mV s^{-1} in 0.1 M phosphate buffer (pH = 7.0) using an Epsilon™ potentiostat/galvanostat (Bioanalytical Systems, Inc., West Lafayette, IN, USA). In the absence of paracetamol, the supporting electrolyte exhibited no electroactive signals (—), confirming that the phosphate medium itself did not contribute to any detectable redox activity. When the system contained 0.5 mM Fe^{2+}, a well-defined oxidation peak at 0.42 V and a corresponding reduction band at 0.30 V were observed, which can be attributed to the Fe^{3+}/Fe^{2+} redox couple (—). In contrast, after 90 min of treatment with the SPEF process (—), the voltammogram displayed a single irreversible oxidation peak centered at 0.44 V. This response is ascribed to the formation of intermediate species that are difficult to detect by HPLC, or to short-chain carboxylic acids complexed with Fe^{3+}, which retain electroactive properties identifiable by cyclic voltammetry [35,36].

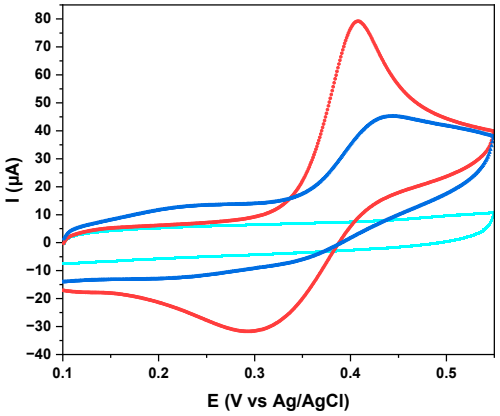

Figure 7. Cyclic voltammogram of 20 mg L^{-1} paracetamol in 0.1 M phosphate buffer with 0.05 mM Fe^{2+} at pH = 7.0 using a scan rate of 100 mV s^{-1}. (—) Supporting electrolyte alone, (—) 0 min of treatment of SPEF, and (—) after 90 min of SPEF treatment at j = 60 mA cm^{-2}.

These results suggest that the degradation of paracetamol under SPEF proceeds through the generation of electroactive by-products that are poorly oxidizable and persist in the solution, thereby explaining the partial mineralization observed at the end of the process.

3.6. COD Removal, ACE Evaluation, and Energy Consumption

To better understand the oxidative capacity of the tested SPEF process, the corresponding solution COD was determined, and the percentage of COD removal was calculated from Equation (14):

$$\%\text{COD removal} = \frac{\Delta(\text{COD})}{\text{COD}_0} 100 \quad (14)$$

where COD_0 is the initial COD value of the solution (in mg O_2 L^{-1}). The average current efficiency (ACE in %) was then estimated according to Equation (15) [37]:

$$\%\ \text{ACE} = \frac{F\ V_s\ \Delta(\text{COD})}{8\ I\ t} 100 \quad (15)$$

where Δ(COD) is expressed in mg O_2 L^{-1}, 8 is the oxygen equivalent mass (in g eq^{-1}), and t is the electrolysis time (in s).

Figure 8A shows that 78% of COD was removed after 90 min of the SPEF process (●), indicating that highly persistent by-products remained in the final treated solution, in agreement with the cyclic voltammetric analysis. Regarding the ACE value (■), the initial value of 15% was progressively slowed down to 8% at 90 min. This decay can be related to two simultaneous effects, the gradual removal of organic load and the production of more hardly oxidizable by-products [38]. The rapid loss of ACE yielded a continuous enhancement of EC_{COD} calculated by Equation (11) with electrolysis time, as shown in Figure 8B. As can be seen, at 90 min, a low EC_{COD} of 0.0519 kWh $(g\ COD)^{-1}$ was obtained, a similar value to that reported by Zhang et al. [39] for tetracycline removal by PEF without considering the energy cost of the UV lamp.

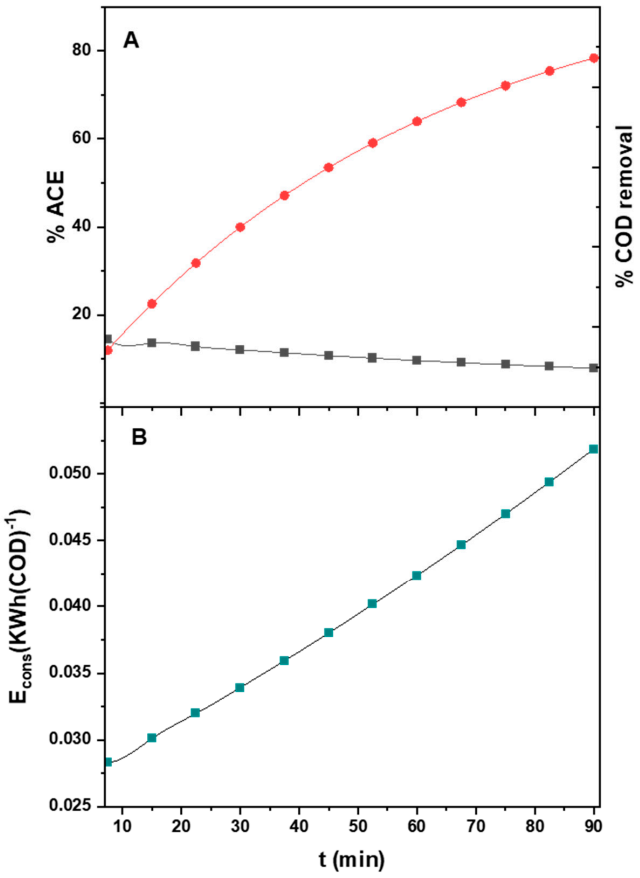

Figure 8. (**A**) Percent of (●) COD removal and (■) average mineralization current vs. electrolysis time and (**B**) energy consumption per unit COD mass for the SPEF process at j = 60 mA cm^{-2}.

3.7. Treatment of a Mixture of Drugs with the Coupled SPEF/Ozone Process

Having established that the SPEF process achieves high degradation efficiencies for paracetamol, the subsequent experiments focused on a multi-component system representative of pharmaceutical mixtures used during the COVID-19 pandemic for symptomatic treatment within the Mexican health system. The selected drugs included dexamethasone, paracetamol, amoxicillin, and azithromycin. Recent studies have reported the persistence and accumulation of these pharmaceuticals in aquatic environments, raising growing environmental concerns. Therefore, exploring effective strategies for their removal is of significant relevance, and this work proposes SPEF as a viable alternative for their degradation [38].

To seek not only the treatment of water contaminated with drugs but also its disinfection, it was decided to carry out tests using ozone. Figure 9 (■) shows the time course of the overall concentration of a mixture of dexamethasone (0.25 mg L^{-1}), paracetamol (50 mg L^{-1}), amoxicillin (50 mg L^{-1}), and azithromycin (16 mg L^{-1}) with 0.05 M Na_2SO_4 at pH = 3.0 by applying 5 L min^{-1} of O_3 flow. The action of this oxidant, combined with sunlight, yielded 34% content removal at 180 min of electrolysis. This decay is higher than 60% for the SPEF/O_3 process (●), indicating the beneficial effect of the generated •OH oxidants on the process. Since paracetamol was removed in less than 90 min (see Figure 4), the other pharmaceuticals tested were much more recalcitrant to oxidation. Regarding the COD decay between 0 and 180 min of electrolysis, 41% was abated, pointing to the remaining part of the drugs and their degradation by-products.

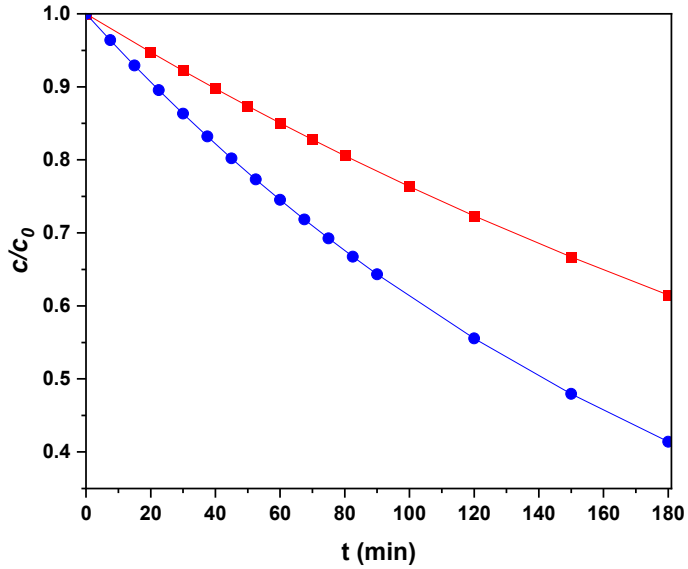

Figure 9. Time course of the normalized total drug concentration for a mixture of dexamethasone (0.25 mg L^{-1}), paracetamol (50 mg L^{-1}), amoxicillin (50 mg L^{-1}), and azithromycin (16 mg L^{-1}) under (■) O_3/sunlight and (●) SFEF/O_3 processes.

It is important to emphasize that the addition of ozone can enhance the degradation of recalcitrant pharmaceuticals, particularly those with an aromatic structure. However, this process may also lead to the formation of aromatic intermediates, which could persist in solution due to their limited susceptibility to attack by the generated reactive oxygen species (ROS). In parallel, the electrocatalytic activity of the electrodes may decrease over the course of electrolysis, potentially as a result of catalyst deactivation by iron poisoning and/or the accumulation of oxidation intermediates formed in situ [40–46].

Based on the results of this research, it is highlighted that the main novelty of this work is the demonstration of the synergistic use of a solar photoelectro-Fenton system

coupled with ozone in a pilot-scale CPC reactor for the efficient degradation of complex mixtures of drugs related to the treatment of COVID-19, which represents a significant advance towards the real implementation of hybrid EAOP technologies for the treatment of water contaminated with pharmaceutical residues.

Further information on kinetic behavior is presented in Tables S1 and S2.

4. Conclusions

The COVID-19 pandemic generated profound consequences worldwide, not only from a public health perspective but also in terms of environmental impact. During the health crisis, medical services relied on the pharmaceutical resources available at that time, including various symptomatic treatments. As a result, numerous therapeutic protocols were implemented in the absence of specific antiviral drugs. However, one of the unintended outcomes has been the emergence of water pollution, since elevated concentrations of these pharmaceuticals have been detected in wastewater effluents across different regions of the world. This occurs because a significant fraction of the administered drugs is not metabolized in the human body and is instead excreted, mainly through urine and sweat. Consequently, the proper treatment of these contaminated water streams represents a pressing challenge for the future.

In this study, the degradation of paracetamol (50 mg L^{-1}) as well as a drug mixture representative of COVID-19 symptomatic treatments—namely dexamethasone (0.25 mg L^{-1}), paracetamol (50 mg L^{-1}), amoxicillin (50 mg L^{-1}), and azithromycin (16 mg L^{-1})—was evaluated using solar photoelectro-Fenton (SPEF) and SPEF combined with ozonation (SPEF/O_3) processes. All experiments were conducted in a pilot plant equipped with a CPC-type photoreactor (30 L working volume) coupled to a filter-press electrochemical cell with a BDD/BDD electrode configuration.

For the SPEF process, complete degradation (100%) of paracetamol was achieved under j = 60 mA cm^{-2}, with a COD removal of 78%, a Faradaic efficiency of η = 8%, and an energy consumption (ECCOD) of 0.0518 kWh $(g\ COD)^{-1}$. In the case of the drug mixture, the SPEF/O_3 system significantly outperformed the standalone O_3/solar process, achieving nearly 60% degradation and 41% COD abatement.

The findings of this research provide a promising perspective toward addressing a real and current environmental challenge. The results demonstrate that electrochemical advanced oxidation processes (EAOPs) coupled with solar irradiation are highly effective for the degradation of complex mixtures of recalcitrant pharmaceuticals, highlighting their potential applicability for large-scale water treatment.

Therefore, the main contribution of this study is to demonstrate experimentally, systematically, and with analytical support that a solar-powered hybrid SPEF/O_3 system is highly effective in the degradation of pharmaceuticals widely used during the COVID-19 pandemic. This innovation focuses not only on technical efficiency but also on its environmental, economic, and social potential, aligning with the principles of sustainability and public health.

This work represents a solid step toward cleaner, more scalable, and more relevant environmental remediation technologies to address the emerging threats of pharmaceutical contamination in wastewater. The use of enriched raw water constitutes an intermediate approach to a real-world system, as it allows for the evaluation of process efficiency under controlled conditions; however, this strategy still has limitations due to the complexity of real-world matrices. Therefore, further research is needed to validate the technology directly in real-world wastewater to confirm its performance, robustness, and applicability in practical treatment scenarios.

Supplementary Materials: The following supporting information can be downloaded at: https://www.mdpi.com/article/10.3390/pr13103234/s1, Figure S1: Estimated logarithmic trend in corticosteroid consumption (2018 index = 100) for 2018–2022; Figure S2: Estimated logarithmic trend in antibiotic consumption (2018 index = 100) for 2018–2022; Figure S3: Estimated logarithmic trend in analgesic consumption (2018 index = 100) for 2018–2022; Table S1: Time course of the normalized total drug concentration for a mixture of dexamethasone (0.25 mg L^{-1}), paracetamol (50 mg L^{-1}), amoxicillin (50 mg L^{-1}), and azithromycin (16 mg L^{-1}) under O_3/sunlight; Table S2: Time course of the normalized total drug concentration for a mixture of dexamethasone (0.25 mg L^{-1}), paracetamol (50 mg L^{-1}), amoxicillin (50 mg L^{-1}), and azithromycin (16 mg L^{-1}) under O_3/SFEF. References cited in Supplementary Materials [47–51].

Author Contributions: Research, data analysis, review and editing, S.H.-C.; Writing, review, editing and conceptualization, M.P.-Á.; Review and editing, L.A.G.; Conceptualization, review and editing, E.B.; Writing, review, conceptualization, data analysis and project management, J.M.P.-H. All authors have read and agreed to the published version of the manuscript.

Funding: This work is supported by the CONAHCYT National Laboratory for Water Science and Technology (LNCyTA), number 101, as the National Laboratory for CONAHCYT, Grant LN-2025-I-16.

Data Availability Statement: The original contributions presented in this study are included in the article. Further inquiries can be directed to the corresponding author.

Acknowledgments: The authors would like to thank the University of Guanajuato for funding this research and Laboratorio Nacional UG-UAA-CONHACyT, Laboratorio Nacional Conahcyt de Ciencia Y Tecnología del Agua (LNCyTA). S.H.-C. thanks the SECIHTI scholarship for the MS degree grant.

Conflicts of Interest: The authors declare no conflicts of interest.

References

1. Tortonese, S.; Scriabine, I.; Anjou, L.; Loens, C.; Michon, A.; Benabdelhak, M.; Ouali, S.; Morin, G.; Laifi, M.; Dobosziewicz, H.; et al. COVID-19 in patients on maintenance dialysis in the Paris region. *Kidney Int. Rep.* **2020**, *5*, 1535–1544. [CrossRef]
2. Noreen, S.; Maqbool, I.; Madni, A. Dexamethasone: Therapeutic potential, risks, and future projection during COVID-19 pandemic. *Eur. J. Pharmacol.* **2021**, *894*, 173854. [CrossRef]
3. Miah, M.S.; Mamun, M.R.; Saif-Ur-Rahman, K.M.; Rabby, A.A.; Zakaria, A.F.M. A qualitative exploration of purchasing, stockpiling, and use of drugs during the COVID-19 pandemic in an urban city of Bangladesh. *Public Health Pract.* **2024**, *7*, 100477. [CrossRef]
4. Mostafa, E.M.A.; Tawfik, A.M.; Abd-Elrahman, K.M. Egyptian perspectives on potential risk of paracetamol/acetaminophen-induced toxicities: Lessons learnt during COVID-19 pandemic. *Toxicol. Rep.* **2022**, *9*, 541–548. [CrossRef]
5. Watanabe, Y.; Nakamura, I.; Sato, S.; Fujita, H.; Kobayashi, T.; Watanabe, H. Comparison of methylprednisolone pulse vs conventional dexamethasone for adult cases of COVID-19 requiring oxygen; a Japanese retrospective cohort study. *J. Infect. Chemother.* **2023**, *29*, 269–273. [CrossRef] [PubMed]
6. Manjani, L.; Desai, N.; Kohli, A.; Arya, R.; Woods, C.; Desale, S. Effects of acetaminophen on outcomes in patients hospitalized with COVID-19. *Chest* **2021**, *160*, A1072. [CrossRef]
7. Albornoz, L.L.; Soroka, V.D.; Silva, M.C.A. Photo-mediated and advanced oxidative processes applied for the treatment of effluents with drugs used for the treatment of early COVID-19: Review. *Environ. Adv.* **2021**, *6*, 100140. [CrossRef]
8. Domingo-Echaburu, S.; Irazola, M.; Prieto, A.; Rocano, B.; Lopez de Torre-Querejazu, A.; Quintana, A.; Orive, G.; Lertxundi, U. Drugs used during the COVID-19 first wave in Vitoria-Gasteiz (Spain) and their presence in the environment. *Sci. Total Environ.* **2022**, *820*, 153122. [CrossRef]
9. Melo, J.R.R.; Duarte, E.C.; de Moraes, M.V.; Fleck, K. Automedicação e uso indiscriminado de medicamentos durante a pandemia da COVID-19. *Cad. Saúde Pública* **2021**, *37*, e00053221. [CrossRef] [PubMed]
10. Agarwal, N. Paracetamol—A contaminant of high concern: Existence in environment and adverse effect. *Pharm. Drug Regul. Aff. J.* **2022**, *5*, 128. [CrossRef]
11. Koagouw, W.; Arifin, Z.; Olivier, G.W.J.; Ciocan, C. High concentrations of paracetamol in effluent dominated waters of Jakarta Bay, Indonesia. *Mar. Pollut. Bull.* **2021**, *169*, 112558. [CrossRef]
12. Miglione, A.; Raucci, A.; Cristiano, F.; Mancini, M.; Gioia, V.; Frugis, A.; Cinti, S. Paper-based 2D configuration for the electrochemical and facile detection of paracetamol in wastewaters. *Electrochim. Acta* **2024**, *488*, 144255. [CrossRef]

13. Garcia-Segura, S.; Brillas, E. Redesigning electrochemical-based Fenton processes: An updated review exploring advances and innovative strategies using phenol degradation as key performance indicator. *Appl. Catal. B Environ.* **2024**, *194*, 206980. [CrossRef]
14. Wang, L.; Jiang, J.; Ma, J.; Pang, S.; Zhang, T. A review on advanced oxidation processes homogeneously initiated by copper (II). *Chem. Eng. J.* **2022**, *427*, 131721. [CrossRef]
15. Jiang, H.; Chen, H.; Duan, Z.; Huang, Z.; Wei, K. Research progress and trends of biochar in the field of wastewater treatment by electrochemical advanced oxidation processes (EAOPs): A bibliometric analysis. *J. Hazard. Mater. Adv.* **2023**, *10*, 100305. [CrossRef]
16. Brillas, E.; Peralta-Hernandez, J.M. The recent development of innovative photoelectro-Fenton processes for the effective and cost-effective remediation of organic pollutants in waters. *Chemosphere* **2024**, *366*, 143465. [CrossRef]
17. Poza-Nogueiras, V.; Arellano, M.; Rosales, E.; Pazos, M.; González-Romero, E.; Sanromán, M.A. Heterogeneous electro-Fenton as plausible technology for the degradation of imidazolinium-based ionic liquids. *Chemosphere* **2018**, *199*, 68–75. [CrossRef] [PubMed]
18. Poza-Nogueiras, V.; Moratalla, A.; Pazos, M.; Sanromán, A.; Sáez, C.; Rodrigo, M.A. Exploring the pressurized heterogeneous electro-Fenton process and modelling the system. *Chem. Eng. J.* **2022**, *431*, 133280. [CrossRef]
19. Nguyen, D.D.D.; Quang, H.H.P.; Nguyen, X.H.; Nguyen, T.P. The treatment of real dyeing wastewater by the electro-Fenton process using drinking water treatment sludge as a catalyst. *RSC Adv.* **2021**, *11*, 27443–27452. [CrossRef] [PubMed]
20. Ganesan, R.; Latha, A.; Venkatesan, G.; Krishnakumari, B. Treatment of textile dyes with steel flakes via Fenton and electro-Fenton processes: An experimental analysis. *Desalination Water Treat.* **2024**, *320*, 100837. [CrossRef]
21. He, Y.; Sutton, N.B.; Rijnaarts, H.H.M.; Langenhoff, A.A.M. Degradation of Paracetamol and Its Oxidation Products in Surface Water by Electrochemical Oxidation. *Environ. Eng. Sci.* **2018**, *35*, 1022–1031. [CrossRef]
22. Xia, Y.; Dai, J.; Yan, Y.; Ma, X.; Feng, H.; Ding, Y. Energy-efficient electrochemical treatment of paracetamol using a PbO_2 anode based on pulse electrodeposition strategy: Kinetics, energy consumption and mechanism. *Environ. Res.* **2022**, *216*, 114673. [CrossRef]
23. Zhang, F.; Li, J.; He, Z. Bio-Electrochemical Degradation of Paracetamol in a Microbial Fuel Cell-Fenton System. *Chem. Eng. J.* **2015**, *276*, 185–192. [CrossRef]
24. Tang, J.; Yao, S.; Xiao, F.; Xia, J.; Xing, X. Electrochemical Oxidation of Landfill Leachate after Biological Treatment by Electro-Fenton System with Corroding Electrode of Iron. *Int. J. Environ. Res. Public Health* **2022**, *19*, 7745. [CrossRef]
25. Moreira, F.C.; Boaventura, R.A.R.; Brillas, E.; Vilar, V.J.P. Electrochemical advanced oxidation processes: A review on their application to synthetic and real wastewaters. *Appl. Catal. B Environ.* **2017**, *202*, 217–261. [CrossRef]
26. Guineo-Salinas, R.; Cotillas, S.; Cañizares, P.; Rodrigo, M.A.; Brillas, E.; Sirés, I. Solar photoelectro-Fenton degradation of nalidixic acid in a pilot plant using a BDD/air-diffusion cell coupled with a CPC photoreactor. *Chem. Eng. J.* **2018**, *333*, 444–453. [CrossRef]
27. Salmerón, I.; García-Gómez, J.; López, F.; López-González, J.A.; Arrebola, F.J.; Quiroga, J.M.; Quiroga, J.M. Treatment of winery wastewater by solar photoelectro-Fenton at a pilot plant. *Catal. Today* **2013**, *209*, 199–204. [CrossRef]
28. Prieto-Rodríguez, L.; Oller, I.; Fernández-Ibáñez, P.; Agüera, A.; Cabrera Reina, A.; Méndez-Arriaga, F.; Maldonado, M.I.; Malato, S. Application of solar photocatalytic ozonation for micropollutant removal in real municipal wastewater effluents. *Appl. Catal. B Environ.* **2013**, *142–143*, 561–569. [CrossRef]
29. Moreira, F.C.; Sousa, J.M.; Macedo, G.; Ribeiro, A.R.; Barreiros, L.; Pedrosa, M.; Faria, J.L.; Gomes, H.T.; Nunes, O.C.; Manaia, C.M.; et al. Photocatalytic ozonation of urban wastewater and surface water pollutants. *Sci. Total Environ.* **2019**, *646*, 734–744. [CrossRef]
30. Kuznetsov, V.V.; Ivantsova, N.A.; Kuzin, E.N.; Pirogov, A.V.; Mezhuev, Y.O.; Filatova, E.A.; Averina, Y.M. Study of the Process of Electrochemical Oxidation of Active Pharmaceutical Substances on the Example of Nitrofurazone ((2E)-2-[(5-Nitro-2-furyl)methylene]hydrazine Carboxamide). *Processes* **2023**, *11*, 3370. [CrossRef]
31. Oturan, N.; Oturan, M.A.; Trellu, C. Comparative Performance of Ten Electrodes in Electro-Fenton Process for Removal of Organic Pollutants from Water. *ChemElectroChem* **2021**, *8*, 3294–3303. [CrossRef]
32. Montenegro-Ayo, R.; Morales-Gomero, J.C.; Alarcón, H.; Corzo, A.; Westerhoff, P.; Garcia-Segura, S. Photoelectrocatalytic Degradation of 2,4-Dichlorophenol in a TiO_2 Nanotube-Coated Disc Flow Reactor. *Chemosphere* **2021**, *268*, 129320. [CrossRef]
33. Martínez-Huitle, C.A.; Panizza, M. Electrochemical oxidation of organic pollutants for wastewater treatment. *Curr. Opin. Electrochem.* **2018**, *11*, 62–71. [CrossRef]
34. Ganiyu, S.O.; Martínez-Huitle, C.A.; Oturan, M.A. Electrochemical advanced oxidation processes for wastewater treatment: Advances in formation and detection of reactive species and mechanisms. *Curr. Opin. Electrochem.* **2021**, *27*, 100678. [CrossRef]
35. Chaplin, B.P. The prospect of electrochemical technologies advancing worldwide water treatment. *Acc. Chem. Res.* **2019**, *52*, 596–604. [CrossRef]
36. Brillas, E. A review on the photoelectro-Fenton process as efficient electrochemical advanced oxidation for wastewater remediation. In *Treatment of Wastewater Using Biological and Chemical Processes*; IntechOpen: London, UK, 2019. [CrossRef]

37. Brillas, E.; Oturan, M.A. Electro-Fenton process and related electrochemical technologies based on Fenton's reaction chemistry. *Chem. Rev.* **2014**, *114*, 2313–2381. [CrossRef] [PubMed]
38. Martínez-Huitle, C.A.; Ferro, S. Electrochemical oxidation of organic pollutants for the wastewater treatment: Direct and indirect processes. *Chem. Soc. Rev.* **2006**, *35*, 1324–1340. [CrossRef]
39. Rodrigo, M.A.; Cañizares, P.; Sánchez-Carretero, A.; Sáez, C. Electrochemical technologies for the regeneration of urban wastewaters. *Electrochim. Acta* **2010**, *55*, 8160–8164. [CrossRef]
40. Anglada, Á.; Urtiaga, A.; Ortiz, I. Contributions of electrochemical oxidation to waste-water treatment: Fundamentals and review of applications. *J. Chem. Technol. Biotechnol.* **2009**, *84*, 1747–1755. [CrossRef]
41. Cañizares, P.; Lobato, J.; Paz, R.; Rodrigo, M.A.; Sáez, C. Electrochemical oxidation of phenolic wastes with boron-doped diamond anodes. *Water Res.* **2005**, *39*, 2687–2703. [CrossRef]
42. Peralta-Hernández, J.M.; Meas-Vong, Y.; Rodríguez, F.J.; Chapman, T.W.; Maldonado, M.I.; Godínez, L.A. In situ electrochemical treatment of wastewater polluted with different azo dyes. *J. Hazard. Mater.* **2006**, *138*, 173–181. [CrossRef]
43. Amado-Pina, D.; Roa-Morales, G.; Barrera-Diaz, C.; Balderas-Hernandez, P.; Romero, R.; Martin del Campo, E.; Natividad, R. Synergic effect of ozonation and electrochemical methods on oxidation and toxicity reduction: Phenol degradation. *Fuel* **2017**, *198*, 82–90. [CrossRef]
44. Mecha, A.C.; Onyango, M.S.; Ochieng, A.; Fourie, C.J.S.; Momba, M.N.B. Synergistic effect of UV–vis and solar photocatalytic ozonation on the degradation of phenol in municipal wastewater: A comparative study. *J. Catal.* **2016**, *341*, 116–125. [CrossRef]
45. Xu, X.; Zhou, X.; Wang, Y.; Wang, X.; Wu, D.; Chen, C. Enhanced photocatalytic ozonation of phenol by Ag/ZnO: Activity, mineralization, and stability. *Catalysts* **2019**, *9*, 1006. [CrossRef]
46. Mecha, A.C.; Onyango, M.S.; Ochieng, A.; Momba, M.N.B. Ultraviolet and solar photocatalytic ozonation of municipal wastewater: Catalyst reuse, energy requirements and toxicity assessment. *Chemosphere* **2017**, *186*, 669–676. [CrossRef]
47. Callaway, K.K.; Tadrous, M.; Kane-Gill, S.L.; Barbash, I.; Rothenberger, S.D.; Suda, K. Changes in Purchases for Intensive Care Medicines during the COVID-19 Pandemic. *Chest* **2021**, *160*, 2123–2134. [CrossRef] [PubMed]
48. Zhou, F.; Deng, J.; Heybati, K.; Zuo, Q.K.; Ali, S.; Hou, W.; Wong, C.Y.; Ramaraju, H.B.; Chang, O.; Dhivagaran, T.; et al. Efficacy and Safety of Corticosteroid Regimens for the Treatment of Hospitalized COVID-19 Patients: A Meta-Analysis. *Future Virol.* **2022**, *17*, 463–489. [CrossRef] [PubMed]
49. Van Paassen, J.; Vos, J.S.; Hoekstra, E.M.; Neumann, K.M.; Boot, K.M.; Arbous, S.M. Corticosteroid Use in COVID-19 Patients: A Systematic Review and Meta-Analysis on Clinical Outcomes. *Crit. Care* **2020**, *24*, 696. [CrossRef] [PubMed]
50. Nandi, A.; Pecetta, S.; Bloom, D. Global Antibiotic Use during the COVID-19 Pandemic: Analysis of Pharmaceutical Sales Data from 71 Countries, 2020–2022. *EClinicalMedicine* **2023**, *57*, 101848. [CrossRef]
51. Tanty, A.; Vitale, E.; Lombardo, D.; Grévy, A.; Gibert, P.; Chapuis, C.; Chevallier Brilloit, C.; Allenet, B.; Bedouch, P.; Chanoine, S. Impact des Soins Pharmaceutiques dans la Prise en Charge des Patients Atteints de COVID-19 en Période de Crise Sanitaire. *Le Pharm. Clin.* **2022**, *57*, 101377. [CrossRef]